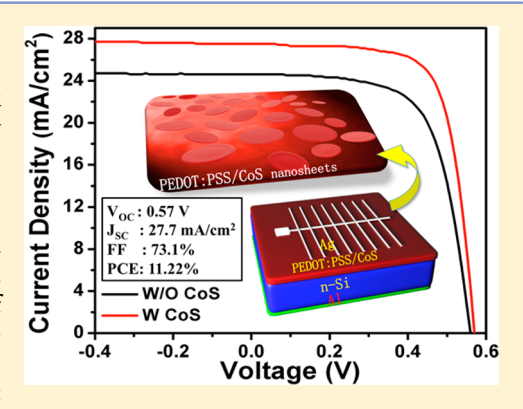
# Two-Dimensional CoS Nanosheets Used for High-Performance Organic—Inorganic Hybrid Solar Cells

Xiao Fang, Tao Song,\* Ruiyuan Liu, and Baoquan Sun\*

Jiangsu Key Laboratory for Carbon-Based Functional Materials & Devices, Institute of Functional Nano & Soft Materials (FUNSOM), and Collaborative Innovation Center of Suzhou Nano Science and Technology, Soochow University, 199 Ren'ai Road, Suzhou, 215123, China

Supporting Information

ABSTRACT: Poly(3,4-ethylenedioxythiophene)/poly(styrenesulfonate) (PEDOT:PSS) is one of the most popular hole-transporting materials in organic—Si hybrid solar cells. However, the inferior sheet resistance and the low work function of the PEDOT:PSS layer hinder the power conversion efficiency (PCE) of the devices. Here, two-dimensional cobalt sulfide (CoS) nanosheets with a low sheet resistance and higher work function are blended into the PEDOT:PSS films in order to enhance the device performance. By tuning the morphology and concentration of CoS nanosheets in the PEDOT:PSS films, a lower recombination rate at the organic—inorganic interfaces and improved hole-transporting ability can be achieved simultaneously, yielding a PCE of 11.2% under simulated air mass 1.5 solar irradiation at 100 mW cm<sup>-2</sup>. The scanning Kelvin probe microscopy, the ultraviolet photoelectron spectroscopy, four-probe sheet resistance measurement, and the transient electrical output



characterization were used to study the origin of performance improvements in devices with CoS nanosheets blended in the PEDOT:PSS films.

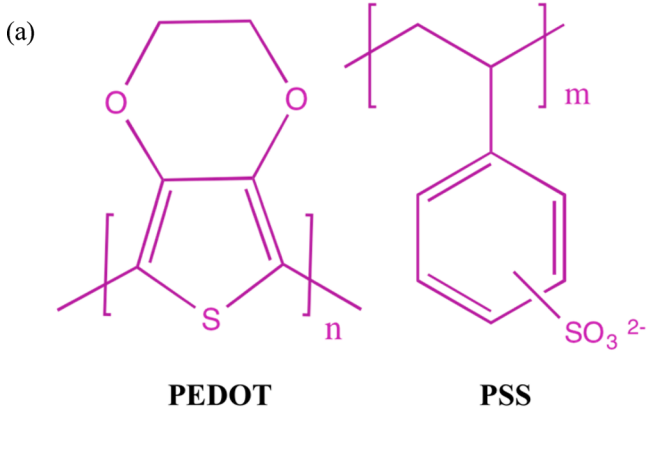
# 1. INTRODUCTION

Since the first introduction of the two-dimensional (2D) atomic crystal graphene, it has been widely studied as a conceptual new class of material in many applications because of its intriguing properties.<sup>1,2</sup> More recently, inspired by the layer structure of graphene, 2D materials have attracted increasing attention due to their unique dimension-dependent properties, such as excellent charge transportation and fewer trap states.<sup>3</sup> Moreover, 2D materials have offered a new access to the lowdimensional research. Among those 2D materials, transitionmetal chalcogenides distinguish themselves by their advantageous electrical properties over the bulk materials. For example, a high mobility of at least 200 cm<sup>2</sup> V<sup>-1</sup> S<sup>-1</sup> at room temperature has been reported in a field effect transistor based on a single layer of molybdenum disulfide (MoS<sub>2</sub>).<sup>4</sup> Solution processed few-layer MoS2 films were used as electron-blocking and holetransporting layers in inverted organic solar cells, yielding a remarkable device performance.<sup>5</sup> A free-standing single-layer tin disulfide was used in visible-light water splitting due to its fast interfacial charge transport.<sup>6</sup> Among these transition-metal chalcogenides, cobalt sulfide (CoS) displays a high conductivity and great electrocatalytic abilities. <sup>7–9</sup> The nanostructured CoS has been successfully applied to different kinds of energy devices, showing promising performances. For instance, CoS nanowires were used in electrochemical capacitors, achieving a specific capacitance as high as 508 F g<sup>-1.7</sup> CoS nanospheres displayed excellent performance as cathode active materials for lithium-rechargeable batteries.8 The CoS nanosheets with a 2D

configuration have been used in dye-sensitized solar cells because of the higher catalytic activity as well as the enlarged surface area for the redox reaction. The CoS/graphene and CoS/multiwalled carbon nanotubes have also been successfully applied to dye-sensitized solar cells. Inspired by the aforementioned applications, it is highly desirable to explore the possibility to use the 2D CoS nanosheets for other optoelectronic devices.

Recently, the economically feasible, cost-effective organic—inorganic hybrid solar cells based on silicon and conjugated polymer have attracted great research interests. 12–26 These devices benefit from the high quality and well-developed fabrication techniques of silicon materials and the facial low-temperature solution process of conjugated organic materials. The water-soluble conductive polymer poly(3,4-ethylenedioxy-thiophene)/poly(styrenesulfonate) (PEDOT:PSS) is widely used in hybrid photovoltaic (PV) devices owing to its excellent features, such as high conductivity, good film-forming properties, and high visible-light transmittance (the chemical structure is shown in Figure 1a). Basically, the typical Si/PEDOT:PSS hybrid solar cells are categorized into the Schottky solar cells in which the PEDOT:PSS layer plays a key role in building up the Schottky junction with n-type silicon (the energy diagram is shown in Figure 1b). 13,28–30 The conductivity of PEDOT:PSS

Received: June 26, 2014 Revised: July 31, 2014 Published: August 8, 2014



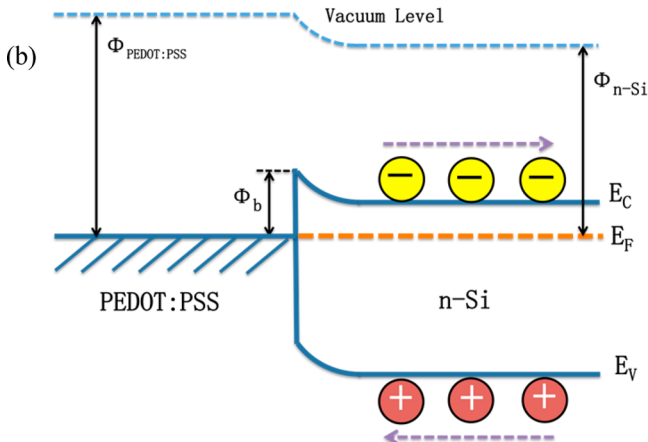


**Figure 1.** (a) Chemical structure of PEDOT and PSS. (b) Energy diagram of Schottky solar cell based on PEDOT:PSS and n-type silicon.  $\Phi_{\text{PEDOT:PSS}}$  and  $\Phi_{\text{n-Si}}$  are the work functions of PEDOT:PSS and n-type silicon, respectively.  $\Phi_{\text{b}}$  is the Schottky barrier height.  $E_{\text{F}}$  is the energy of the Fermi level.  $E_{\text{C}}$  and  $E_{\text{V}}$  are the conduction band and valence band, respectively.

directly determines the hole collection property in the hybrid devices. However, the sheet resistance of PEDOT:PSS films is still inferior to that of the commonly used transparent electrodes, such as indium tin oxide and aluminum doped zinc oxide, which limits the hole transport and the overall device performance of hybrid solar cells. Meanwhile, by tuning the work function of the organic layers and controlling the interface property of the silicon surfaces, there is still some space to increase the built-in potential in the hybrid solar cells. Recently, these limitations have been conquered in different kinds of ways. For instance, by adding the organic solvent such as dimethyl sulfoxide (DMSO) into the PEDOT:PSS solution, the insulating PSS segregation shells can be reduced at the surface of the PEDOT:PSS grains. The conductivity of the PEDOT:PSS films can be dramatically increased from 0.2 to 99 S/cm, improving the performance of Si/PEDOT:PSS hybrid solar cells.<sup>17</sup> The perfluorinated ionomer (PFI) was also introduced in the PEDOT:PSS films to increase the work function of the hole-transporting layer and enhance the built-in potential in the hybrid solar cells. In the PFI blended polymer films, a considerable work function increase of 0.3 eV was obtained. Finally, a power conversion efficiency (PCE) of 9.9% was achieved, which was 20% higher than that of the control devices without PFI additive.<sup>29</sup>

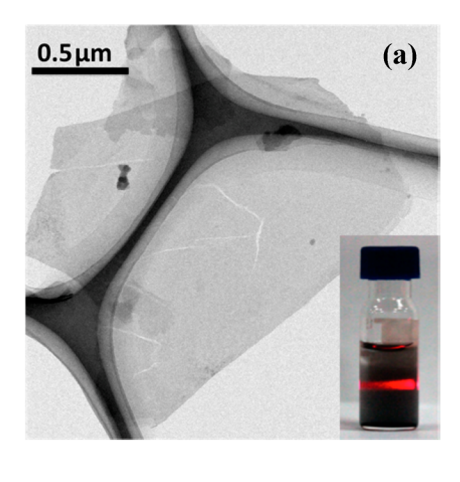
In this study, we employed the CoS nanosheets to enhance the conductivity and deepen the work function of PEDOT:PSS layers in order to improve the PV performances of the hybrid silicon solar cells. The conductivity of PEDOT:PSS with and without CoS nanosheets was measured by a four-probe method. Scanning Kelvin probe microscopy (SKPM) and ultraviolet photoelectron spectroscopy (UPS) have been used to further explore the work function change of the PEDOT:PSS films in the presence of CoS nanosheets. It is found that the device with the CoS nanosheets blended PEDOT:PSS layers achieved a PCE of 11.2%, which was 18.6% higher than that of the pristine ones without CoS nanosheets.

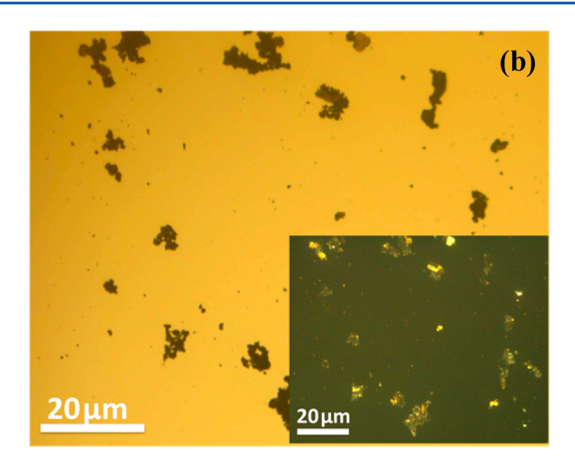
#### 2. EXPERIMENTAL SECTION

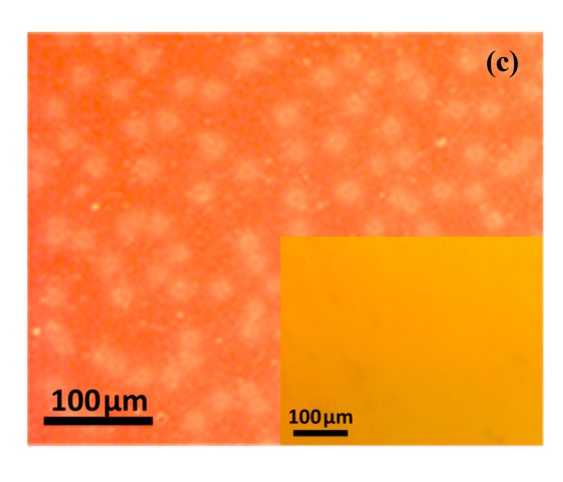
**2.1. Synthesis of CoS Nanosheets.** The synthesis of CoS nanosheets was adapted from a typical hydrothermal method. A 20 mL portion of 0.1 M cobalt nitrite aqueous solution was dropped into 20 mL of 0.1 M thiourea aqueous solution with vigorous stirring at room temperature. After stirring for about 20 min, 0.1 M hexamethylenetetramine aqueous solution was added into the above solution. Then, the solution was transferred into a Teflon-lined autoclave and kept at 180 °C for 24 h. The resultant product was obtained by centrifuging at 3000 rpm and then washed with deionized (DI) water and ethanol, subsequently. This wash process was repeated three times to completely remove the unreacted chemicals and byproducts. Finally, CoS powder was dried in a vacuum oven at 80 °C for 3 h.

**2.2. Device Fabrication.** One-side-polished n-type 0.9–1.3  $\Omega$ -cm Si (100) wafers were methylated through a two-step chlorination/alkylation process. 31,32 Triton (1 wt %) (Sigma-Aldrich) and DMSO (5 wt %) were mixed in highly conductive PEDOT:PSS solution (CLEVIOS PH 1000). The solid content of the PEDOT:PSS solution is ~1.2%. The as-synthesized CoS was dispersed into the PEDOT:PSS solution with concentrations of 0.05, 0.10, 0.15, and 0.20 mg/mL, respectively. The weight ratio between PEDOT:PSS and CoS for its optimized device performance is about 120:1. The mixed solution was kept stirring for about 2 h. PEDOT:PSS solution was spincoated on the silicon substrate at 2000 rpm for 1 min and subsequently sintered at 125 °C for 0.5 h under a nitrogen atmosphere. A silver grid electrode was deposited on the PEDOT:PSS layer. The Al back contact was deposited by a vacuum thermal evaporator.

2.3. Characterization. The PV characterization was conducted in an ambient environment. A Newport 91160 solar simulator equipped with a 300 W xenon lamp and an air mass (AM) 1.5 filter was used to generate the simulated solar spectrum irradiation source. The irradiation intensity was 100 mW/cm<sup>2</sup> calibrated by a Newport standard silicon solar cell 91150. The edges of the devices were covered with aluminum foil, and the area for illumination was 1 cm  $\times$  0.8 cm. A Newport monochromator 74125 and power meter 1918 with silicon detector 918D were used in the external quantum efficiency (EQE) measurements. All of the electrical data were recorded by a Keithley 2612 sourcemeter. The morphology was observed through an FEI Tecnai G2 F20 STWIN transmission electron microscope (TEM). The transient photovoltage measurements were conducted under white bias light with intensities ranging from 0.1 to 1 sun generated by a lightemitting diode (LED). The green laser light source from a laser diode (532 nm, 30-200 mW, Kingbright) triggered by a functional signal generator provided a square-wave modulated







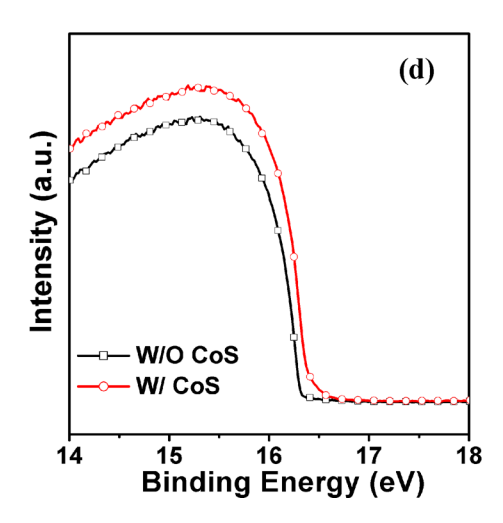


Figure 2. (a) TEM image of the CoS nanosheets. The inset shows that the corresponding colloidal ethanol dispersion displays the Tyndall effect. (b) Optical microscope image of CoS on silicon substrate. The inset image shows the CoS film under a birefringent microscope. (c) Optical microscope image of the CoS/PEDOT:PSS film. The optical microscope image of a pristine PEDOT:PSS film is also shown in the inset. (d) The UPS spectra of PEDOT:PSS films with and without CoS.

illumination, leading to a small ( $\sim$ 10 mV) perturbation voltage. The photovoltage and photocurrent signals were recorded by a Tektronix oscilloscope. UPS measurements were performed in a KRATOS ULTRA-DLD ultra-high-vacuum surface analysis system. The spectra were measured by using an unfiltered HeI (21.22 eV) gas discharge lamp and a total instrumental energy resolution of 100 meV. X-ray diffraction (XRD) measurement was carried out using an X-ray powder diffractometer (PANAlytical Empyrean).

# 3. RESULTS AND DISCUSSION

**3.1.** Analysis of PEDOT:PSS Films Mixed with CoS Nanosheets. The crystal structure of CoS nanosheets obtained by one-step hydrothermal reaction was examined by XRD. As shown in Figure S1 (Supporting Information), the diffraction peaks can be indexed to CoS, matching well with its standard XRD pattern (Jaipurite CoS 75-0605). The TEM image of the CoS nanosheets is shown in Figure 2a, revealing the compact layer structure of the CoS nanosheets. The high-resolution transmission electron microscopy (HRTEM) image and selected area electron diffraction (SAED) pattern of the CoS nanosheets are shown in Figure S2a,b (Supporting Information), which indicates its high crystalinity. When these CoS nanosheets were dispersed in ethanol, the Tyndall

effect can be easily observed (Figure 2a, inset), indicating a good dispersion capability. Figure 2b shows the optical microscope image of the sheetlike CoS on a silicon substrate. In the polarized light mode, the shape of CoS nanosheets is clearly visible because of the birefringent property (shown in Figure 2b, inset), which indicates that the as-synthesized CoS has a good crystal quality. In addition, according to the different brightness of the CoS nanosheets, they should be few-layer (~3–4 layers) instead of single-layer.

Regarding CoS nanosheets synthesized by hydrothermal reaction, a possible mechanism can be expected to explain the CoS nucleation and growth, as shown below:

$$Co^{2+} + 2C_6H_{12}N_4 \rightarrow [Co(C_6H_{12}N_4)_2]^{2+}$$
 (1)

$$[Co(C_6H_{12}N_4)_2]^{2+} + S^{2-} \rightarrow CoS + 2C_6H_{12}N_4$$
 (2)

The cobalt ions first react with hexamethylenetetramine to form relatively stable cobalt complexes of  $[\text{Co}(\text{C}_6\text{H}_{12}\text{N}_4)_2]$ . The cobalt complexes further react with sulfur ions, which are slowly released from thiourea to form CoS nanosheets. Therefore, there may be some organic ligands of hexamethylenetetramine attaching on the CoS nanosheets. In order to verify this point, the infrared spectroscopy measurement of the CoS nanosheet and hexamethylenetetramine were conducted,

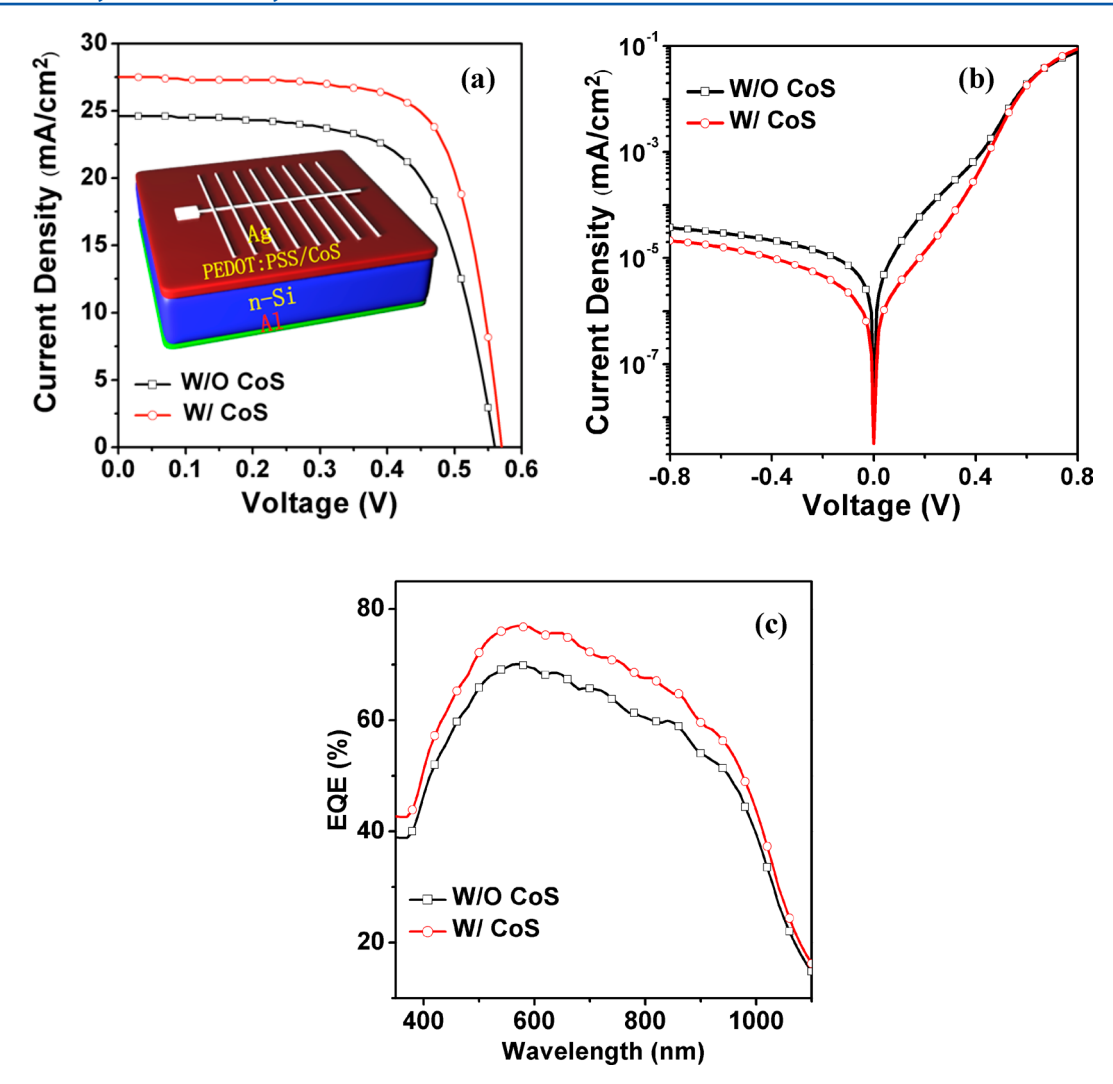


Figure 3. (a) Electric output characteristics of Schottky solar cells based on n-Si and PEDOT:PSS with and without 0.10 mg/mL CoS under AM 1.5 light with the intensity of 100 mW/cm². The schematic graph of the device structure is shown in the inset. (b) Dark-current—voltage curves and (c) EQE spectra of the devices with and without 0.10 mg/mL CoS.

respectively, as shown in Figure S3 (Supporting Information). Both spectra show vibrating peaks (2850-3000 cm<sup>-1</sup>) for carbon-hydrogen bonds and peaks of (1000-1350 cm<sup>-1</sup>) for carbon-nitrogen bonds, which indicates that there is hexamethylenetetramine residue on the surface of the CoS nanosheets. According to the zeta potential measurement results, the CoS nanosheet displays a slight surface positive charge, which originates from hexamethylenetetramine molecules. In the PEDOT:PSS solution, the conductive PEDOT grains are surrounded by the insulating PSS shells. The chemical structures of PEDOT and PSS are illustrated in Figure 1a. The PSS counterion is used in PEDOT synthesis to form a stable dispersion. At the same time, for PEDOT with a positive charge, the polyanion PSS is required to form a polyelectrolyte complex. However, the PSS shell at the PEDOT grain surface acts as a barrier for charge transport. The CoS nanosheet with a positive charge can be easily adhered onto the PSS shell that presents a negative charge. The interaction between the CoS nanosheet and PEDOT:PSS enhances their compatibility, as shown in Figure S4 (Supporting Information). Meanwhile, the distribution of CoS nanosheets in the solid films of PEDOT: PSS is very uniform, reflecting a good dispersivity of CoS in the PEDOT:PSS solution, as shown in Figure 2c.

The organic-inorganic hybrid device is based on the Schottky junction between PEDOT:PSS and n-Si, as shown in Figure 1b. PEDOT:PSS was a transparent window electrode with a good light transparency (300-1100 nm, >90%). Here, a silver grid electrode was deposited onto the PEDOT:PSS to improve hole collection efficiency. The generated photocurrent originates from the light harvesting of c-Si. Both the conductivity and work functions of the transparent electrodes play key roles in the PV performance of hybrid silicon solar cells. 17,23,28,29,33 Therefore, the conductivity of the PEDOT: PSS films with and without CoS was characterized by a fourprobe method. Since all the films were fabricated at the same condition, the thicknesses of different films were almost identical (~100 nm) as measured by an ellipsometry. By the four-probe method, each film was measured at 10 different positions in order to evaluate the film resistivity accurately. The square resistivity of the pristine PEDOT:PSS film was slightly decreased from 196 to 180  $\Omega/\Box$  when PEDOT:PSS was mixed with 0.1 mg/mL CoS nanosheets. We believe that the sheet resistivity reduction of the conductive polymer film mixed with CoS nanosheets should be ascribed to the high charge carrier transport properties of CoS nanosheets.

Table 1. Parameters Extracted from the I-V Curves of Devices with or without CoS<sup>a</sup>

devices	$J_{\rm SC}~({\rm mA/cm^2})$	$V_{\rm OC}$ (V)	FF (%)	PCE (%)
W/O CoS	24.6	0.56	68.5	9.46
	$(24.5 \pm 0.10)$	$(0.56 \pm 0.00)$	$(67.5 \pm 0.01)$	$(9.27 \pm 0.19)$
W/CoS	27.7	0.57	73.1	11.22
	$(27.4 \pm 0.30)$	$(0.57 \pm 0.00)$	$(72.8 \pm 0.30)$	$(11.07 \pm 0.15)$

<sup>&</sup>lt;sup>a</sup>Data and statistics based on 10 cells of each type. Numbers in bold are the maximum recorded values. Numbers in italic are the average recorded values.

The work function of PEDOT:PSS films with and without CoS was also investigated by both SKPM and UPS measurements. For n-type silicon contacting with PEDOT:PSS layers, the built-in potential  $(V_{bi})$  increases when the work function of PEDOT:PSS grows. The enhanced  $V_{\rm bi}$  can supply a higher driving force to sweep the light-induced charge carrier out of the junction region, improving the PV performances of solar cells. In order to quantitatively study the work function change by incorporating CoS, the surface potential of the PEDOT:PSS layers was probed by SKPM measurement.34,35 The relation between work function of the conductive tip  $(\varphi_t)$  and the sample  $(\varphi_s)$  can be described by the equation  $\varphi_s = \varphi_t - eV_{CPD}$ , where e is the elementary charge and  $V_{\mathrm{CPD}}$  is the surface potential directly measured by SKPM. The work function variation can be easily observed by comparing the difference of  $V_{\text{CPD}}$ . It can be seen from Figure S5 (Supporting Information) that, in the PEDOT:PSS films blended with 0.10 mg/mL CoS nanosheets, the  $V_{\rm CPD}$  was  ${\sim}{-300}$  mV, while the  $V_{\rm CPD}$  of a pure PEDOT:PSS layer was  $\sim$  120 mV. The  $V_{\rm CPD}$  of the composite film decreased ~180 mV, indicating a corresponding increase of the work function.

In order to further confirm the positive shift of work function, UPS analysis was also performed. The work function of the PEDOT:PSS film can be evaluated by abstracting the cutoff value from the excitation source of 21.22 eV. As shown in Figure 2d, the work function of the composite film shifted to a more negative value (4.96 eV) compared with the pristine one (4.8 eV). This shift is consistent with the SKPM measurement results

**3.2. Photovoltaic Performance.** In order to explore the effect of CoS in hybrid silicon solar cells, devices were fabricated with different amounts of CoS additive (0, 0.05, 0.10, 0.15, 0.20 mg/mL CoS in PEDOT:PSS solution).The schematic diagram of the device structure based on n-Si and PEDOT:PSS is presented in Figure 3a, inset. The device performance was first enhanced by increasing the concentration of CoS in PEDOT:PSS from pristine to the optimal value of 0.1 mg/mL (Figure S6, Supporting Information). The open-circuit voltage  $(V_{OC})$  and fill factor (FF) finally dropped down steeply if the CoS amount exceeded the optimal proportion, possibly due to the device shorting problem caused by the big clusters of CoS nanosheets in the organic hole-transporting layers. Figure 3a shows the current density-voltage (J-V) characteristics of the devices with 0.1 mg/mL or without CoS in the dark and under air mass 1.5 simulated solar light irradiation at 100 mW cm<sup>-2</sup>. The electric output characteristics of short-circuit current density  $(J_{SC})$ ,  $V_{OC}$ , FF, and PCE are summarized in Table 1. The device with 0.1 mg/mL CoS in PEDOT:PSS showed a  $J_{SC}$ of 27.4 mA/cm<sup>2</sup>, an  $V_{\rm OC}$  of 0.57 V, and a FF of 73.1%, resulting in a PCE of 11.2%. Meanwhile, the pristine device without CoS exhibited an efficiency of 9.46% with a  $J_{SC}$  of 24.6 mA/cm<sup>2</sup>, an  $V_{\rm OC}$  of 0.56 V, and a FF of 68.5%. The higher FF and  $I_{\rm SC}$ achieved in the device with CoS were mainly attributed to the

improved hole-transporting property of the conductive polymer layers. The  $J_{\rm SC}$  increment from 24.6 to 27.4 mA/cm² was consistent with the integrated current values from the EQE spectra (Figure 3c).

The slightly improved  $V_{\rm OC}$  is ascribed to the increase of  $V_{\rm bi}$  across the PEDOT:PSS/n-Si junction, because the  $V_{\rm bi}$  is directly proportional to the  $V_{\rm OC}$ . It is known that the  $V_{\rm bi}$  is related to the Schottky junction barrier height  $(\Phi_{\rm b})$ , as shown in the equation  $q\Phi_{\rm b}=qV_{\rm bi}+(E_{\rm C}-E_{\rm F})$ , where  $E_{\rm C}$  is the energy of the conduction band and  $E_{\rm F}$  is the energy of the Fermi level. In the model of a Schottky junction,  $\Phi_{\rm b}$  is determined by the work function of the PEDOT:PSS film  $(W_{\rm PEDOT:PSS})$  and the electron affinity of the semiconductor Si  $(\chi_{\rm Si})$  via the equation  $\Phi_{\rm b}=W_{\rm PEDOT:PSS}-\chi_{\rm Si}$ . Accordingly, the increased  $W_{\rm PEDOT:PSS}$  due to the addition of CoS could increase the  $\Phi_{\rm b}$  in the hybrid solar cells, leading to a higher measured  $V_{\rm OC}$ .

Besides the evidence of a positive  $V_{\rm OC}$  shift under light irradiation, the I-V data measured in the dark were also analyzed in order to further confirm the increase of  $\Phi_h$ . The dark I-V curves of the devices with and without CoS are plotted in Figure 3b. After fitting the I-V curves by the equation  $I = I_S \exp[(e(V-IR_S))/(nkT)]$ , the series resistance  $(R_S)$ , the reverse leakage current  $(I_S)$ , and the ideality factor (n)of the devices with and without the CoS were extracted, respectively. The device with CoS exhibited a lower  $I_s$  of 9.05  $\times$  $10^{-9}$  mA/cm<sup>2</sup> and a smaller  $R_S$  of 0.87  $\Omega$ ·cm<sup>2</sup> than those of the reference device (1.69  $\times$  10<sup>-7</sup> mA/cm<sup>2</sup>, 1.54  $\Omega$ ·cm<sup>2</sup>). It was observed that the reverse leakage current  $(I_s)$  was suppressed significantly when CoS was added, indicating the decrease of recombination processes in the space charge region owing to the higher barrier caused by CoS. In order to further verify this point, the  $\Phi_b$  was calculated on the basis of the following equation<sup>36</sup>

$$I = I_{S} \left[ \exp \left( \frac{eV}{nkT} \right) - 1 \right]$$
$$= AA * T^{2} \exp \left( -\frac{\Phi_{b}}{kT} \right) \left[ \exp \left( \frac{eV}{nkT} \right) - 1 \right]$$

where A is the contact area,  $A^*$  is the effective Richardson constant ( $\approx$ 252 A cm<sup>-2</sup> k<sup>-2</sup> for n-type silicon), T is the absolute temperature, e is the electronic charge, and k is the Boltzmann constant. According to the calculation results, in the devices with the optimal concentration of CoS nanosheets in PEDOT:PSS, the  $\Phi_b$  increased from 0.83 to 0.91 eV. Meanwhile, the ideality factor of the pristine device exhibited a larger value of 1.897 compared with 1.523 of the device based on CoS/PEDOT:PSS. The reduction of the n value reveals the important role of CoS in decreasing the charge recombination and improving the junction quality.

To further confirm the beneficial effect of CoS nanosheets in the hybrid solar cells, the transient electric output characteristics were measured.  $^{37-39}$  The photovoltage decay measure-

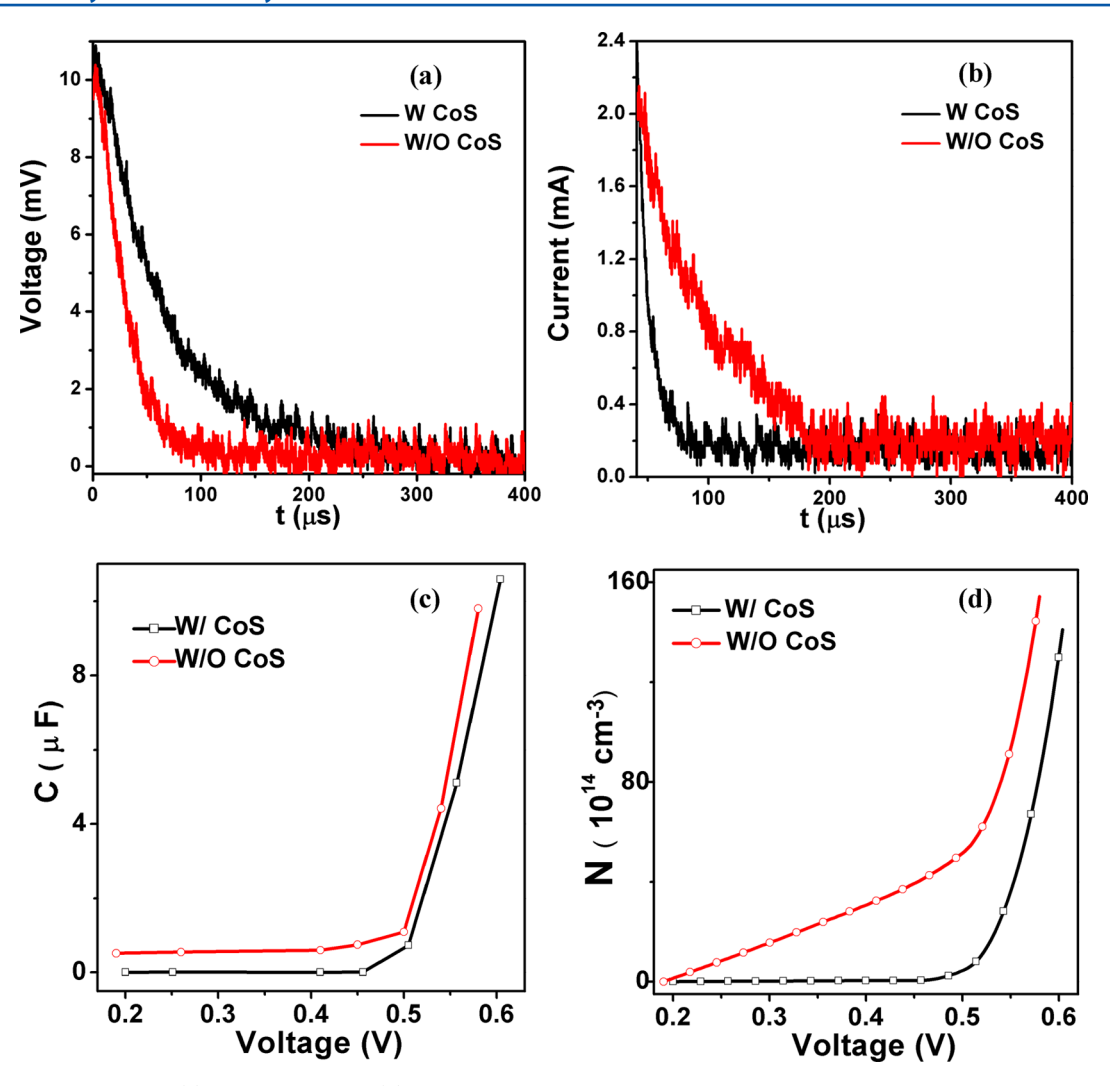


**Figure 4.** Typical time-resolved (a) photovoltage and (b) photocurrent decay curves of the hybrid devices with and without CoS nanosheets biased by white light irradiation and excited under a laser light pulse perturbation. (c) The differential capacitances C and (d) the carrier concentration N at the different  $V_{\rm OC}$  of the hybrid silicon solar cells with or without CoS.

ments were conducted at open-circuit condition, as shown in Figure 4a. The photocurrent transient decay measurements were conducted by connecting the PV devices in series with a 50 ohm resistor, as shown in Figure 4b. Steady-state photovoltage with a value varying from 0 V to  $V_{\rm OC}$  was obtained under different bias light intensities. When the devices were exposed to the short laser pulse, a certain amount of photogenerated charge carriers were injected immediately, leading to a temporary increase of charge carrier density. The transient photocurrent decay was used to determine the differential charge density, from which the carrier concentration (N) could be estimated. When a small amount of charge  $\Delta Q$ was injected to the device, the differential capacitance (C) can be obtained by recording the transient decay curves of both photocurrent and photovoltage. The  $\Delta Q$  and C can be calculated by  $\Delta Q = \int_0^t I \, dt$  and  $C = \Delta Q/\Delta V_0$ , respectively, where I is the transient photocurrent,  $\Delta V_0$  is the maximum transient voltage ( $\sim$ 10 mV),  $\Delta Q$  is the charge obtained by integrating the photocurrent transient with respect to time (t)for the same laser pulse, and C is the capacitance at each  $V_{\rm OC}$ . At last, the carrier concentration N can be acquired by integrating the capacitance over steady-state photovoltage,

which can be described by  $N = (1/Aed) \int_0^{Voc} C \, dV$ , where d is the device thickness.

At open-circuit condition, the measurement of photovoltage decay opens a window for probing the recombination in the device. The laser pulse perturbation leads to the transient decay of photovoltage. A fast decay of photovoltage stands for the fast recombination. In Figure 4a, a 2-fold increase in decay time can be observed when there are CoS nanosheets in the PEDOT: PSS layer. We believe that the CoS nanosheets adhered on the PEDOT grains reduced the energy barrier caused by the PSS shell, resulting in a more efficient charge transport. By connecting the device in series with a 50  $\Omega$  resistor, the photocurrent decay was measured simultaneously under the same laser perturbation as used in the photovoltage decay measurement. A small amount of additional charge carriers were injected into the device caused by the light pulse. The  $\Delta Q$ was calculated by integrating the photocurrent decay curve with respect to time. A higher  $\Delta Q$  showed that more charge carriers were blocked in the device. In Figure 4b, the fast decay of photocurrent in the device with CoS can be understood in that the charge carriers were efficiently separated and collected. As shown in Figure 4c, the device without CoS exhibited a higher capacitance than the one with CoS. Similarly, in Figure 4d,

which plots the N vs  $V_{\rm OC}$ , the device with CoS displayed a lower carrier concentration. It is known that, in the bulk of the junction, the stored charge can be described as carrier concentration. On the other hand, the carrier concentration is in proportion to the trap state density. Therefore, the lower carrier concentration indicated that there were fewer trap states and fewer charge recombination processes in the device based on PEDOT:PSS blended with CoS nanosheets, resulting in more efficient hole transport and better PV performances.

## 4. CONCLUSIONS

In summary, we demonstrated that CoS nanosheets can dramatically enhance the performance of Si/PEDOT:PSS hybrid PV devices, yielding a champion PCE of 11.2%. CoS nanosheets can improve the conductivity and deepen the work function level of PEDOT:PSS films, which enhances the hole transport and increases the built-in potential in the Si/PEDOT: PSS devices. The transient electric measurement indicated that the charge recombination can be suppressed in the presence of CoS nanosheets. Our results show that the unique 2D transition-metal chalcogenides materials like CoS could be employed to further improve the PV performance of hybrid silicon solar cells.

#### ASSOCIATED CONTENT

# **S** Supporting Information

The XRD pattern, the HRTEM, and SAED pattern of CoS, the infrared spectra, the cartoon model of CoS in PEDOT:PSS film, the comparison of different CoS concentrations in PEDOT:PSS, and the SKPM images are shown in the Supporting Information. This material is available free of charge via the Internet at http://pubs.acs.org.

#### AUTHOR INFORMATION

### **Corresponding Authors**

\*Tel: 0086-512-65884530. E-mail: tsong@suda.edu.cn (T.S.). \*Tel: 0086-512-65880951. E-mail: bqsun@suda.edu.cn (B.S.).

#### Notes

The authors declare no competing financial interest.

## ACKNOWLEDGMENTS

This work was supported by the National Basic Research Program of China (973 Program) (2012CB932402) and the National Natural Science Foundation of China (61176057, 91123005, 60976050), and the Priority Academic Program Development of Jiangsu Higher Education Institutions.

# REFERENCES

- (1) Novoselov, K. S.; Geim, A. K.; Morozov, S.; Jiang, D.; Zhang, Y.; Dubonos, S.; Grigorieva, I.; Firsov, A. Electric Field Effect in Atomically Thin Carbon Films. *Science* **2004**, *306*, *666*–*669*.
- (2) Novoselov, K. S.; Fal, V.; Colombo, L.; Gellert, P.; Schwab, M.; Kim, K. A Roadmap for Graphene. *Nature* **2012**, *490*, 192–200.
- (3) Xu, M.; Liang, T.; Shi, M.; Chen, H. Graphene-like Two-Dimensional Materials. *Chem. Rev.* 2013, 113, 3766–3798.
- (4) Radisavljevic, B.; Radenovic, A.; Brivio, J.; Giacometti, V.; Kis, A. Single-Layer MoS<sub>2</sub> Transistors. *Nat. Nanotechnol.* **2011**, *6*, 147–150.
- (5) Gu, X.; Cui, W.; Li, H.; Wu, Z.; Zeng, Z.; Lee, S. T.; Zhang, H.; Sun, B. A Solution-Processed Hole Extraction Layer Made from Ultrathin MoS<sub>2</sub> Nanosheets for Efficient Organic Solar Cells. *Adv. Energy Mater.* **2013**, *3*, 1262–1268.
- (6) Sun, Y.; Cheng, H.; Gao, S.; Sun, Z.; Liu, Q.; Liu, Q.; Lei, F.; Yao, T.; He, J.; Wei, S. Freestanding Tin Disulfide Single-Layers Realizing

- Efficient Visible-Light Water Splitting. *Angew. Chem., Int. Ed.* **2012**, *51*, 8727–8731.
- (7) Bao, S.-J.; Li, C. M.; Guo, C.-X.; Qiao, Y. Biomolecule-Assisted Synthesis of Cobalt Sulfide Nanowires for Application in Supercapacitors. *J. Power Sources* **2008**, *180*, 676–681.
- (8) Wang, J.; Ng, S. H.; Wang, G.; Chen, J.; Zhao, L.; Chen, Y.; Liu, H. Synthesis and Characterization of Nanosize Cobalt Sulfide for Rechargeable Lithium Batteries. *J. Power Sources* **2006**, *159*, 287–290.
- (9) Sudhagar, P.; Nagarajan, S.; Lee, Y.-G.; Song, D.; Son, T.; Cho, W.; Heo, M.; Lee, K.; Won, J.; Kang, Y. S. Synergistic Catalytic Effect of a Composite (CoS/PEDOT:PSS) Counter Electrode on Triiodide Reduction in Dye-Sensitized Solar Cells. *ACS Appl. Mater. Interfaces* **2011**, *3*, 1838–1843.
- (10) Das, S.; Sudhagar, P.; Nagarajan, S.; Ito, E.; Lee, S. Y.; Kang, Y. S.; Choi, W. Synthesis of Graphene-CoS Electro-catalytic Electrodes for Dye Sensitized Solar Cells. *Carbon* **2012**, *50*, 4815–4821.
- (11) Xiao, Y.; Wu, J.; Lin, J.-Y.; Tai, S.-Y.; Yue, G. Pulse Electrodeposition of CoS on MWCNT/Ti as a High Performance Counter Electrode for a Pt-Free Dye-Sensitized Solar Cell. *J. Mater. Chem. A* **2013**, *I*, 1289–1295.
- (12) Erickson, A. S.; Zohar, A.; Cahen, D. n-Si—Organic Inversion Layer Interfaces: A Low Temperature Deposition Method for Forming a p—n Homojunction in n-Si. *Adv. Energy Mater.* **2014**, DOI: 10.1002/aenm.201301724.
- (13) Jeong, S.; Garnett, E. C.; Wang, S.; Yu, Z.; Fan, S.; Brongersma, M. L.; McGehee, M. D.; Cui, Y. Hybrid Silicon Nanocone—Polymer Solar Cells. *Nano Lett.* **2012**, *12*, 2971—2976.
- (14) Shen, X.; Sun, B.; Liu, D.; Lee, S.-T. Hybrid Heterojunction Solar Cell Based on Organic–Inorganic Silicon Nanowire Array Architecture. *J. Am. Chem. Soc.* **2011**, *133*, 19408–19415.
- (15) Chen, T.-G.; Huang, B.-Y.; Liu, H.-W.; Huang, Y.-Y.; Pan, H.-T.; Meng, H.-F.; Yu, P. Flexible Silver Nanowire Meshes for High-Efficiency Microtextured Organic-Silicon Hybrid Photovoltaics. *ACS Appl. Mater. Interfaces* **2012**, *4*, 6857–6864.
- (16) Liu, Q.; Ono, M.; Tang, Z.; Ishikawa, R.; Ueno, K.; Shirai, H. Highly Efficient Crystalline Silicon/Zonyl Fluorosurfactant-Treated Organic Heterojunction Solar Cells. *Appl. Phys. Lett.* **2012**, *100*, 183901.
- (17) Pietsch, M.; Bashouti, M. Y.; Christiansen, S. The Role of Hole Transport in Hybrid Inorganic/Organic Silicon/Poly(3,4-ethylene-dioxy-thiophene):Poly(styrenesulfonate) Heterojunction Solar Cells. *J. Phys. Chem. C* **2013**, *117*, 9049–9055.
- (18) Zhang, F.; Liu, D.; Zhang, Y.; Wei, H.; Song, T.; Sun, B. Methyl/Allyl Monolayer on Silicon: Efficient Surface Passivation for Silicon-Conjugated Polymer Hybrid Solar Cell. ACS Appl. Mater. Interfaces 2013, 5, 4678–4684.
- (19) He, L.; Jiang, C.; Wang, H.; Lai, D. Si Nanowires Organic Semiconductor Hybrid Heterojunction Solar Cells toward 10% Efficiency. ACS Appl. Mater. Interfaces 2012, 4, 1704–1708.
- (20) Shiu, S.-C.; Chao, J.-J.; Hung, S.-C.; Yeh, C.-L.; Lin, C.-F. Morphology Dependence of Silicon Nanowire/Poly(3,4-ethylene-dioxythiophene):Poly(styrenesulfonate) Heterojunction Solar Cells. *Chem. Mater.* **2010**, 22, 3108–3113.
- (21) Jeong, H.; Song, H.; Pak, Y.; Kwon, I. K.; Jo, K.; Lee, H.; Jung, G. Y. Enhanced Light Absorption of Silicon Nanotube Arrays for Organic/Inorganic Hybrid Solar Cells. *Adv. Mater.* **2014**, *26*, 3445–3450
- (22) Pietsch, M.; Jäckle, S.; Christiansen, S. Interface Investigation of Planar Hybrid n-Si/PEDOT:PSS Solar Cells with Open Circuit Voltages up to 645 mV and Efficiencies of 12.6%. *Appl. Phys. A: Mater. Sci. Process.* **2014**, *115*, 1109–1113.
- (23) Thomas, J. P.; Leung, K. T. Defect-Minimized PEDOT:PSS/Planar-Si Solar Cell with Very High Efficiency. *Adv. Funct. Mater.* **2014**, DOI: 10.1002/adfm.201400380.
- (24) Pudasaini, P. R.; Ruiz-Zepeda, F.; Sharma, M.; Elam, D.; Ponce, A.; Ayon, A. A. High Efficiency Hybrid Silicon Nanopillar—Polymer Solar Cells. *ACS Appl. Mater. Interfaces* **2013**, *5*, 9620—9627.

- (25) Schmidt, J.; Titova, V.; Zielke, D. Organic-Silicon Heterojunction Solar Cells: Open-Circuit Voltage Potential and Stability. *Appl. Phys. Lett.* **2013**, *103*, 183901.
- (26) Moiz, S. A.; Nahhas, A. M.; Um, H.-D.; Jee, S.-W.; Cho, H. K.; Kim, S.-W.; Lee, J.-H. A Stamped PEDOT:PSS—Silicon Nanowire Hybrid Solar Cell. *Nanotechnology* **2012**, *23*, 145401.
- (27) Ouyang, J.; Xu, Q.; Chu, C.-W.; Yang, Y.; Li, G.; Shinar, J. On the Mechanism of Conductivity Enhancement in Poly(3,4-ethylene-dioxythiophene):Poly(styrene sulfonate) Film Through Solvent Treatment. *Polymer* **2004**, *45*, 8443–8450.
- (28) Shen, X.; Zhu, Y.; Song, T.; Lee, S.-T.; Sun, B. Hole Electrical Transporting Properties in Organic-Si Schottky Solar Cell. *Appl. Phys. Lett.* **2013**, *103*, 013504.
- (29) Zhu, Y.; Song, T.; Zhang, F.; Lee, S.-T.; Sun, B. Efficient Organic-Inorganic Hybrid Schottky Solar Cell: The Role of Built-In Potential. *Appl. Phys. Lett.* **2013**, *102*, 113504.
- (30) Liu, Q.; Khatri, I.; Ishikawa, R.; Fujimori, A.; Ueno, K.; Manabe, K.; Nishino, H.; Shirai, H. Improved Photovoltaic Performance of Crystalline-Si/Organic Schottky Junction Solar Cells Using Ferroelectric Polymers. *Appl. Phys. Lett.* **2013**, *103*, 163503.
- (31) Bashouti, M. Y.; Stelzner, T.; Christiansen, S.; Haick, H. Covalent Attachment of Alkyl Functionality to 50 nm Silicon Nanowires through a Chlorination/Alkylation Process. *J. Phys. Chem.* C 2009, 113, 14823–14828.
- (32) Haick, H.; Hurley, P. T.; Hochbaum, A. I.; Yang, P.; Lewis, N. S. Electrical Characteristics and Chemical Stability of Non-Oxidized, Methyl-Terminated Silicon Nanowires. *J. Am. Chem. Soc.* **2006**, *128*, 8990—8991.
- (33) Huang, J.; Miller, P. F.; Wilson, J. S.; de Mello, A. J.; de Mello, J. C.; Bradley, D. D. Investigation of the Effects of Doping and Post-Deposition Treatments on the Conductivity, Morphology, and Work Function of Poly(3,4-ethylenedioxythiophene)/Poly(styrene sulfonate) Films. *Adv. Funct. Mater.* **2005**, *15*, 290–296.
- (34) Sun, L.; Wang, J.; Bonaccurso, E. Nanoelectronic Properties of a Model System and of a Conjugated Polymer: A Study by Kelvin Probe Force Microscopy and Scanning Conductive Torsion Mode Microscopy. *J. Phys. Chem. C* **2010**, *114*, 7161–7168.
- (35) Palermo, V.; Palma, M.; Samorì, P. Electronic Characterization of Organic Thin Films by Kelvin Probe Force Microscopy. *Adv. Mater.* **2006**, *18*, 145–164.
- (36) Sze, S. M.; Ng, K. K. Physics of Semiconductor Devices; John Wiley & Sons: Hoboken, NJ, 2006.
- (37) Ip, A. H.; Thon, S. M.; Hoogland, S.; Voznyy, O.; Zhitomirsky, D.; Debnath, R.; Levina, L.; Rollny, L. R.; Carey, G. H.; Fischer, A. Hybrid Passivated Colloidal Quantum Dot Solids. *Nat. Nanotechnol.* **2012**, *7*, 577–582.
- (38) Shuttle, C.; O'Regan, B.; Ballantyne, A.; Nelson, J.; Bradley, D.; Durrant, J. Bimolecular Recombination Losses in Polythiophene: Fullerene Solar Cells. *Phys. Rev. B* **2008**, *78*, 113201.
- (39) Li, Z.; Gao, F.; Greenham, N. C.; McNeill, C. R. Comparison of the Operation of Polymer/Fullerene, Polymer/Polymer, and Polymer/Nanocrystal Solar Cells: A Transient Photocurrent and Photovoltage Study. *Adv. Funct. Mater.* **2011**, *21*, 1419–1431.